Experimental study of non-inductive current in Heliotron J

Gen MOTOJIMA, Kazunobu NAGASAKI[1], Hiroyuki OKADA[1], Kiyomasa WATANABE,
Tohru MIZUUCHI[1], Akinobu Matsuyama[2], Kiyoshi HANATANI[1], Satoshi YAMAMOTO[1],
Shinji KOBAYASHI[1], Yasuhiro SUZUKI, Katsumi KONDO[2], Yuji NAKAMURA[2],
Angela C. FERNÁNDEZ[3], Álvaro A. CAPPA[3], Yasuo YOSHIMURA, Shinya WATANABE[2],
Kiyofumi Mukai[2] and Fumimichi SANO[1]

National Institute for Fusion Science, Toki 509-5292, Japan
[1] *Institute of Advanced Energy, Kyoto University, Uji 611-0011, Japan*
[2] *Graduate School of Energy Science, Kyoto University, Uji 611-0011, Japan*
[3] *Laboratorio Nacional de Fusión, EURATOM-CIEMAT, Madrid 28040, Spain*

It is important to control non-inductive current for generation and steady-state operation of high-performance plasmas in toroidal fusion devices. Helical devices allow dynamic control of non-inductive current through a wide variety of magnetic configurations. The reversal of non-inductive current consisting of bootstrap current and electron cyclotron driven current in electron cyclotron heating plasmas has been observed in a specific configuration at low density in Heliotron J device. By analyzing the non-inductive current for normal and reversed magnetic fields, we present experimental evidence for the reversal of bootstrap current. Our experiments and calculations suggest that the reversal is caused by a positive radial electric field of about 10 kV/m. Moreover, we show that the typical electron cyclotron current drive efficiency in Heliotron J plasma is about 1.0×10^{17} AW^{-1}m^{-2}, which is comparable to other helical devices. We have found that the value is about 10 times lower than that of tokamak devices. This might be due to an enhanced Ohkawa effect by trapped particles.

Keywords: bootstrap current, ECCD, Heliotron J, trapped particle

1. Introduction

Non-inductive current has a potential to permit a steady-state operation and improve a plasma performance in toroidal fusion devices. Steady-state operation is attained by a large fraction of non-inductive current in tokamak devices. In helical devices, non-inductive current can modify magnetohydrodynamic (MHD) equilibrium and stability by changing the rotational transform profile [1, 2]. Moreover, helical devices allow dynamic control of non-inductive current through a wide variety of magnetic configurations. In Heliotron J, a low-magnetic-shear helical-axis heliotron device, the dependence of non-inductive current such as bootstrap current and electron cyclotron (EC) driven current on the magnetic configuration has been investigated [3–5]. Additionally, the effect of non-inductive current on the rotational transform has been studied by measurement of MHD activities [6].

In Heliotron J, calculation of bootstrap current using the neoclassical theory (SPBSC code [7]) reveals that the bootstrap current depends on the bumpiness of the Fourier components in Boozer coordinates [3,8]. This dependence can be explained qualitatively by the change in the direction of $\mathbf{B} \times \nabla B$. In off-axis electron cyclotron heating (ECH) plasmas in which the bootstrap current dominates, the measured non-inductive current is in good agreement with the neoclassical calculation except for low bumpiness configuration at low density [4]. The direction of the measured non-inductive current is opposite to the theoretical one. Here, the radial electric field is not included in the calculation. Although we assume that the discrepancy is due to the reversal of bootstrap current by a positive radial electric field and/or non-negligible electron cyclotron current drive (ECCD), we do not clarify the reason for the occurrence of the reversal in low bumpiness configuration. One of the objectives of this study is to investigate the characteristics of non-inductive current in low bumpiness configuration at low density.

EC driven current occurs via two mechanisms: (1) the Fisch-Boozer effect [9] by passing particles, and (2) the Ohkawa effect [10] by trapped particles. The direction of current driven by the Fisch-Boozer effect is opposite to that driven by the Ohkawa effect, and the direction of the total current is determined by the balance between them. In Heliotron J, the direction of EC driven current is reversed by the magnetic ripple structure [5], probably because the ripple structure changes the fraction of trapped particles. In tokamak devices, the reduction of off-axis ECCD efficiency has been observed, which is explained by the effect of trapped particles [11]. Off-axis ECCD is recognized as

a useful tool for suppressing MHD modes such as the neoclassical tearing mode. Therefore, it is important to understand the effect of trapped particles on ECCD in toroidal fusion devices. The other objective of this study is to evaluate the ECCD efficiency in Heliotron J, and to compare it with that in tokamak devices.

The rest of the paper is organized as follows. The experimental setup is described in Section 2. In Section 3, the experimental results for the bootstrap current and EC driven current are discussed. In Section 4, we discuss the effect of a radial electric field on the bootstrap current. In addition, the difference in ECCD efficiency between Heliotron J and tokamak devices is discussed. We present the conclusions in Section 5.

2. Experimental Setup

Heliotron J is a medium-sized helical-axis heliotron device with a major radius (R) of 1.2 m and an average plasma minor radius (a) of 0.1-0.2 m. The coil system consists of an $L = 1$, $M = 4$ continuous helical coil, two sets of toroidal coils, and three pairs of vertical coils. Here, L is the pole number of the helical coil, and M is the pitch number of the field along the toroidal direction. The confinement configuration is composed of four "straight" sections and four "corner" sections. A wide variety of magnetic configurations can be formed by these external coils. Bumpiness, $\epsilon_\mathrm{b}(= B_{04}/B_{00})$, is introduced as a third knob to control the neoclassical transport in addition to the other major field harmonics in Boozer coordinates, helicity (B_{14}/B_{00}) and toroidicity (B_{10}/B_{00}). Here, B_mn is the Fourier component with the poloidal and toroidal mode numbers of m and n, respectively. Plasmas are produced and heated by a 70 GHz second harmonic X-mode ECH with a power of 350 kW. The waves are injected perpendicularly with respect to the equatorial plane. However, a finite parallel refractive index of 0.44 at magnetic axis lies in these experiments because of the three-dimensional magnetic structure, and thereby EC driven current can be produced

In ECH plasmas, non-inductive current has two components: bootstrap current and EC driven current. Total non-inductive current is measured by Rogowski coils. In this study, positive (negative) non-inductive current is defined as co-(counter-)direction, i.e., having a direction increasing (decreasing) the inherent rotational transform. We can control the contribution of the bootstrap current and ECCD to non-inductive current by changing the magnetic field strength, ω_0/ω [5]. Here, ω_0 means the electron cyclotron frequency on the axis in the straight section and ω means the injected wave frequency. When the magnetic field is set to $\omega_0/\omega = 0.50$, EC driven current flows weakly due to the off-axis resonance

from the Doppler shift. On the other hand, the EC driven current is higher than the bootstrap current at $\omega_0/\omega = 0.49$ in low density owing to the on-axis resonance.

3. Results

We evaluate the bootstrap current and EC driven current by comparing the non-inductive current obtained for the normal and reversed magnetic field. The direction of the bootstrap current is fixed with the magnetic field direction for the normal and reversed magnetic field, while the direction of the EC driven current reverses because of its association with the magnetic field direction. The non-inductive current for the normal magnetic field, $I_\mathrm{p}^\mathrm{norm}$, can be expressed as

$$I_\mathrm{p}^\mathrm{norm} = I_\mathrm{BS} + I_\mathrm{EC}^\mathrm{norm}, \tag{1}$$

where I_BS is the bootstrap current, and $I_\mathrm{EC}^\mathrm{norm}$ is the EC driven current for the normal magnetic field. The non-inductive current for the reversed magnetic field, $I_\mathrm{p}^\mathrm{rev}$, is expressed as

$$I_\mathrm{p}^\mathrm{rev} = I_\mathrm{BS} + I_\mathrm{EC}^\mathrm{rev}, \tag{2}$$

where $I_\mathrm{EC}^\mathrm{rev}$ is the EC driven current for the reversed magnetic field. If $I_\mathrm{EC}^\mathrm{norm} = -I_\mathrm{EC}^\mathrm{rev}$ is satisfied under the assumption that the plasmas of the normal and reversed magnetic fields are identical, then from Eqs. (1) and (2), the bootstrap current and EC driven current are expressed as follows,

$$I_\mathrm{BS} = \frac{I_\mathrm{p}^\mathrm{norm} + I_\mathrm{p}^\mathrm{rev}}{2}, \tag{3}$$

$$I_\mathrm{EC}^\mathrm{norm} = \frac{I_\mathrm{p}^\mathrm{norm} - I_\mathrm{p}^\mathrm{rev}}{2}. \tag{4}$$

3.1 Bootstrap current and ECCD in low bumpiness configuration

In Ref. [4], it is shown that the direction of non-inductive current in a low bumpiness configuration ($\epsilon_\mathrm{b} = 0.01$) is changed from co- to counter-direction as the electron density decreases. The total non-inductive current is 0.3 kA at $\bar{n}_\mathrm{e} = 1.0 \times 10^{19}$ m^{-3} and it is -0.5 kA at $\bar{n}_\mathrm{e} = 0.4 \times 10^{19}$ m^{-3} at normal magnetic field. In contrast, the non-inductive current flows in the co-direction at any density in medium ($\epsilon_\mathrm{b} = 0.06$) and high bumpiness ($\epsilon_\mathrm{b} = 0.15$) configurations. Here, the magnetic field is set to $\omega_0/\omega = 0.50$. The experiments for the normal and reversed magnetic fields were carried out in ECH plasmas with low bumpiness configuration in order to reveal the contribution of bootstrap current and EC driven current to the reversal of non-inductive current.

Figure 1 shows the dependence of non-inductive current on electron density in the low bumpiness configuration. The electron density is scanned in the
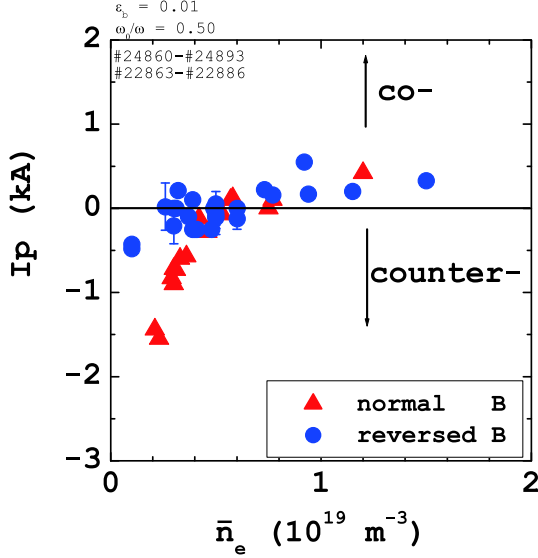
Fig. 1 Density dependence of measured non-inductive current at $\epsilon_b = 0.01$ configuration for normal (triangles) and reversed (circles) magnetic fields.
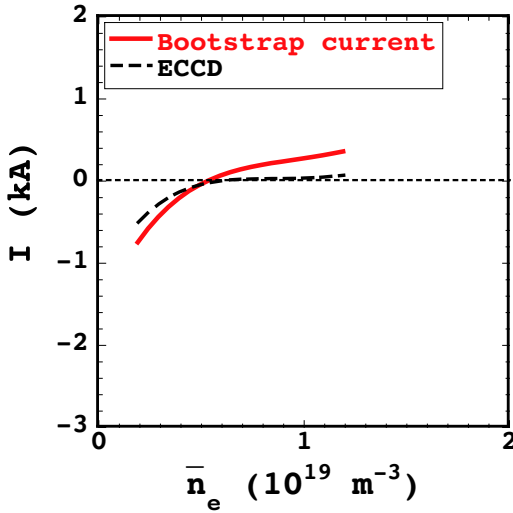

Fig. 2 Density dependence of estimated bootstrap current (solid line) and EC driven current (dashed line).

range from $\bar{n}_e = 0.1 \times 10^{19}$ m^{-3} to $\bar{n}_e = 1.5 \times 10^{19}$ m^{-3}. We confirmed that the stored energies in the normal and reversed magnetic fields are almost same, and therefore, it is assumed that the plasmas for the normal and reversed magnetic fields are identical. The non-inductive current flows in the counter-direction at low density for both cases. A maximum current of -1.6 kA is observed in the normal magnetic field.

The density dependence of the bootstrap and EC driven currents evaluated using Eqs. (3) and (4) are shown in Fig. 2. Here, the polynomial fitting to the data of normal and reversed magnetic field is applied in Fig. 1. The magnitude of the bootstrap current at low density is similar to that of the EC driven current.

It is noted that the direction of the bootstrap current is reversed with decreasing electron density. Bootstrap current of 0.8 kA flows in the counter-direction. The characteristics of the bootstrap current in the counter-direction at low density will be discussed in Section 4.

3.2 ECCD efficiency

Various expressions for ECCD efficiency have been used [12]. In this study, the following figure of merit is adopted

$$\gamma = \frac{n_e I_{EC} R}{P_{EC}} \ (\text{AW}^{-1}\text{m}^{-2}), \tag{5}$$

where P_{EC} is the absorbed ECH power. In Heliotron J, the EC power deposition position can be changed from ripple top to ripple bottom by increasing the bumpiness. Here, the magnetic ripple structure is expressed by the ratio of the magnetic field strength at the straight section where the EC wave is injected (B_{st}) to the magnetic field strength at the corner section (B_{cor}), $h = B_{st}/B_{cor}$. Figure 3 shows the ECCD efficiency as a function of the electron density for three typical magnetic field ripple cases. Here, the magnetic field is set to $\omega_0/\omega = 0.49$. A positive sign of γ denotes ECCD is driven in the direction of the Fisch-Boozer effect, and a negative sign denotes the direction of the Ohkawa effect. γ changes its direction from positive to negative as the ripple structure changes. γ is about 1.0×10^{17} AW^{-1}m^{-2} at ripple top heating ($h = 1.06$) except at low density, while γ at ripple bottom heating ($h = 0.82$), it is almost -0.16×10^{17} AW^{-1}m^{-2}. The reason for the degradation of γ at low density remains unclear. The reversal experiment demonstrates that the Ohkawa effect is enhanced as h decreases. In W7-AS, the reversal of EC driven current at a magnetic ripple structure has been observed [12]. The EC driven current flowing in the direction of the Ohkawa effect is about 10 % of that flowing in the direction of the Fisch-Boozer effect in W7-AS. Therefore, it is found that a ripple structure can control the direction of the ECCD by the effects of trapped particles.

4. Discussion
4.1 The effect of radial electric field on bootstrap current

In Fig. 2, it is shown that the negative bootstrap current is observed for $\bar{n}_e < 0.6 \times 10^{19}$ m^{-3}. In this section, we discuss the physical mechanism of negative bootstrap current at low density. In an ECH plasma at low density, electrons are presumably in a more collisionless regime compared with ions, and the collisionality regimes of electrons and ions are considered to be different. Thus, electrons are more easily lost than ions, and a positive radial electric field can be generated. This is the so-called "electron root". A positive radial electric field has been observed in
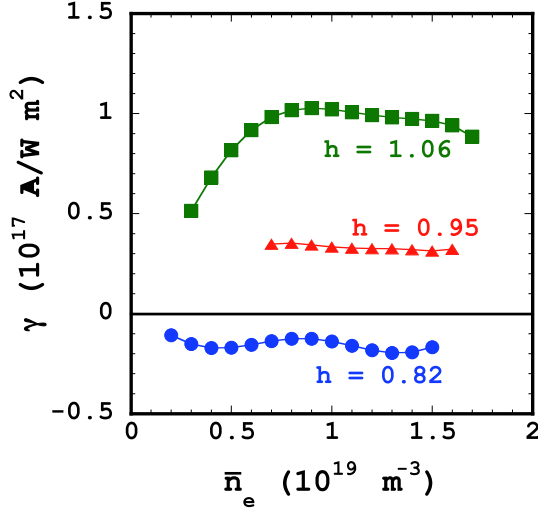
Fig. 3 ECCD efficiency, γ as a function of electron density for three magnetic ripple cases. A positive sign indicates the direction of the Fisch-Boozer effect, and a negative sign indicates the direction of the Ohkawa effect. The ripple top configuration ($h = 0.82$) is equivalent to the low bumpiness ($\epsilon_b = 0.01$) configuration, and the ripple bottom configuration ($h = 1.06$) is equivalent to the high bumpiness ($\epsilon_b = 0.15$) configuration.
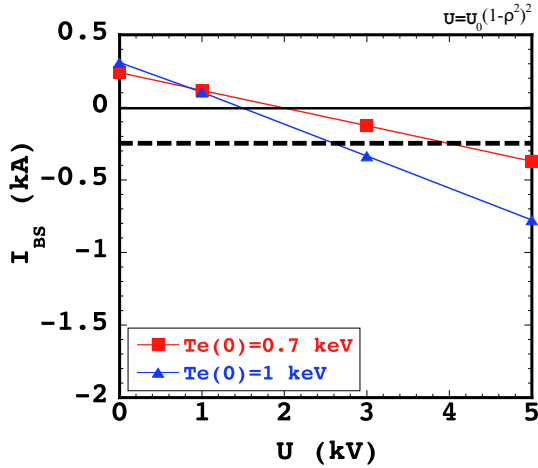

Fig. 4 Dependence of the bootstrap current on the radial electric field for the low bumpiness configuration at low density. Dashed line denotes the experimental value of bootstrap current at $\bar{n}_e = 0.4 \times 10^{19}$ m^{-3}. It is noted that the evaluation of bootstrap current in this study is more accurate than that performed in ref. [4].

helical devices [14–17]. According to the neoclassical theory, a bootstrap current proportional to the radial electric field is predicted in non-axisymmetric devices, when electrons and ions are in different collisionality regimes [18]. The neoclassical theory predicts that the bootstrap current density, j_{bs}, is expressed by [7] under the assumption that electrons are in $1/\nu$ regime and ions are in plateau regime

$$
\begin{aligned}
\langle j_{bs}B \rangle &= \hat{L}_1 \left(G_{bs}^e p_e' + G_{bs}^i p_i' \right) \\
&\quad - \hat{L}_1 (G_{bs}^e - G_{bs}^i) e n_e U' \\
&\quad - \hat{L}_{2e} G_{bs}^e n_e T_e' + \hat{L}_{2i} G_{bs}^i n_e T_i', \quad (6)
\end{aligned}
$$

where the prime means differentiation with respect to the toroidal flux. $\hat{L}_1, \hat{L}_{2e}, \hat{L}_{2i}$ are the coefficients, G is a geometric factor that depends on the magnetic configuration, p is the plasma pressure, U is the electric potential, and T is the temperature. If, for example, electrons are in the $1/\nu$ regime and ions are in plateau regime, then $G_{bs}^e - G_{bs}^i < 0$ and $U' < 0$ are satisfied. Therefore, the term concerning the electric field, $-\hat{L}_1 (G_{bs}^e - G_{bs}^i) e n_e U'$, is negative, inducing a negative bootstrap current.

To investigate the effect of a radial electric field, the bootstrap current calculation considering the radial electric field was carried out using SPBSC code. Figure 4 shows the dependence of the bootstrap current on the radial electric field. The profiles of electron temperature, electron density and radial electric field are assumed to be $n_e = n_0(1 - \rho^6)$, $T_e = T_0(1 - \rho^2)^2$, and $U = U_0(1 - \rho^2)^2$, respectively, because they have not yet been obtained. Figure 4 indicates that if a central electric potential of 2.5-4.0 kV is generated, we can explain the reversal of the bootstrap current. A central potential from 2.5 to 4.0 kV corresponds to an electric field on the order of 10 kV/m, comparable to the electric field experimentally observed in helical devices [14, 15]. Potential measurements will be needed in future.

4.2 Comparison of ECCD efficiency with tokamak devices

In this study, it is shown that the typical ECCD efficiency, γ is about on the order of 10^{17} in Heliotron J. The ECCD efficiency in other medium-sized helical devices (TJ-II and CHS) has been investigated [19]. Table 1 shows the ECCD efficiency in three helical devices. As described in [19], their magnetic field structures differ; however, the magnitude of the EC driven current is a few kA, and the ECCD efficiency is comparable within a factor of 2. Additionally, we now compare our results with ECCD efficiency on tokamaks (DIII-D [20], JT-60U [21], TCV [22]) in Table 1. The ECCD efficiency in tokamaks is about on the order of 10^{18}. The ECCD efficiency in helical devices is about one-tenth that of tokamaks. This is probably due to the enhanced Ohkawa effect from trapped particles. In helical systems, the effect of trapped particles on ECCD is considered to be strong compared with tokamaks, since ripple structure such as bumpiness, helicity and toroidicity are formed in helical system. In general, the helicity and the toroidicity are zero at the magnetic axis. However, the radial drift

Table 1 ECCD efficiency in Heliotron J, DIII-D, JT-60U, TCV.

	Heliotron J	TJ-II	CHS	DIII-D	JT-60U	TCV
Major Radius	1.2 m	1.5 m	1.0 m	1.7 m	3.5 m	0.88 m
Mode	2nd X	2nd X	2nd X	2nd X	1st O	2nd X
EC power	350 kW	300 kW × 2	300 kW	1 MW	1 MW	500 kW × 2
I_{EC}	4.6 kA	2.0 kA	6.0 kA	92 kA	185 kA	100 kA
γ_{EC} $(AW^{-1}m^{-2})$	$\sim 1.0 \times 10^{17}$	$\sim 0.9 \times 10^{17}$	1.6×10^{17}	2.4×10^{18}	5.0×10^{18}	1.7×10^{18}

of trapped particles from the magnetic surface occurs, resulting that the trapped particles have an effect on the ECCD efficiency even in on-axis heating. Furthermore, the EC power deposition has a finite radial width. Therefore, even if the EC power is deposited on-axis, we have to take into account the trapped particle effect on ECCD efficiency. However, the effect of each ripple on the contribution to the Ohkawa effect remains unclear. A ray tracing calculation code considering the trapped particles is under development, and we will clarify the effect of the trapped particles on ECCD quantitatively in future.

5. Conclusions

Non-inductive current experiments were conducted in Heliotron J. Magnetic field reversal experiments revealed that the direction of the bootstrap current is changed from co- to counter-direction with decreasing electron density in the low bumpiness configuration. The reversal is presumably due to the reduction of the bootstrap current attributed to a positive radial electric field. We calculated the bootstrap current considering the radial electric field, and found that a radial electric field on the order of 10 kV/m is required to explain the reversal of the bootstrap current. We plan potential measurements by heavy ion beam probe and/or charge-exchange recombination spectroscopy. The ECCD efficiency, $\gamma = n_e I_{EC} R / P_{EC}$, was evaluated in Heliotron J. The sign of γ changes from positive to negative as the EC power deposition position becomes deeper in the ripple bottom. It is suggested that the effect of trapped particles on ECCD is strong in Heliotron J. The typical efficiency is about 1.0×10^{17} $AW^{-1}m^{-2}$ at ripple top heating ($h = 1.06$). We compared the Heliotron J device with tokamak cases. The ECCD efficiency is about 10 times lower than those in tokamak devices. This may be due to the enhanced Ohkawa effect resulting from trapped particles.

[1] E. Sallander *et al.*, Nucl. Fusion **40**, 1499 (2000).
[2] S. Sakakibara *et al.*, Plasma Fusion Res. **1**, 003 (2006).
[3] G. Motojima *et al.*, J. Korean Phys. Soc. **49**, S87 (2006).
[4] G. Motojima *et al.*, Fusion Sci. Technol. **51**, 122 (2007).
[5] G. Motojima *et al.*, Nucl. Fusion **47**, 1045 (2007).
[6] G. Motojima *et al.*, Plasma Fusion Res. **3**, S1067 (2008).
[7] K. Y. Watanabe *et al.*, Nucl. Fusion **35**, 335 (1995).
[8] Y. Nakamura *et al.*, Fusion Sci. Technol. **50**, 281 (2006).
[9] N. J. Fisch and A. H. Boozer, Phys. Rev. Lett. **45**, 720 (2980).
[10] T. Ohkawa, General Atomics Report GA-A13847 (1976).
[11] T. Suzuki *et al.*, Nucl. Fusion **44**, 699 (2004).
[12] R. Prater, Phys. Plasmas **11**, 2349 (2004).
[13] V. Erckmann and U. Gasparino, Plasma Phys. Control. Fusion **36**, 1869 (1994).
[14] K. Kondo *et al.*, Rev. Sci. Instrum. **59**, 1533 (1988).
[15] A. Fujisawa *et al.*, Phys. Rev. Lett. **82**, 2669 (1999).
[16] K. Ida *et al.*, Phys. Rev. Lett. **86**, 5297 (2001).
[17] H. Maaβberg *et al.*, Phys. Plasmas **7**, 295 (2000).
[18] N. Nakajima and M. Okamoto, J. Phys. Soc. Jpn. **61**, 833 (1992).
[19] K. Nagasaki *et al.*, Plasma. Fusion Res. **3**, S1008 (2008).
[20] T. C. Luce *et al.*, Phys. Rev. Lett. **83**, 4550 (1999).
[21] T. Suzuki *et al.*, Plasma Phys. Control. Fusion **44**, 1 (2002).
[22] O. Sauter *et al.*, Phys. Rev. Lett. **84**, 3322 (2000).